International Journal of Heat and Mass Transfer 133 (2019) 561–571

Contents lists available at ScienceDirect

International Journal of Heat and Mass Transfer

journal homepage: www.elsevier.com/locate/ijhmt

Analytical solution for filmwise condensation in confined high-aspect ratio geometry

Jia Liu [a,b,*], Roman O. Grigoriev [b]

[a] Key Laboratory of Low-grade Energy Utilization Technologies and Systems of Ministry of Education, College of Energy and Power Engineering, Chongqing University, Chongqing 400044, China
[b] School of Physics, Georgia Institute of Technology, Atlanta, GA 30332-0430, USA

ARTICLE INFO

Article history:
Received 25 June 2018
Received in revised form 8 October 2018
Accepted 21 December 2018
Available online 29 December 2018

Keywords:
Filmwise condensation
Noncondensables
Thermocapillary effect

ABSTRACT

This study revisits the problem of free vapor condensation in the filmwise regime by constructing and solving a comprehensive transport model that describes heat and mass transport through the gas phase, interfacial and thermal resistance of the condensate film, and heat conduction through the cooled wall in a self-consistent manner. We have shown that it is possible to obtain an analytical solution of the model which describes the net condensation flux in the presence of an arbitrary amount of noncondensables. This solution demonstrates that the overall thermal resistance reduces to a sum of the thermal resistances of the wall, the condensate film, the interfacial resistance, and the diffusive resistance of the gas layer only in the limit of infinite thermal resistance of the gas layer, but generally has a more complicated form. Finally, we derived an analytical solution for the condensate film thickness profile which generalizes Nusselt's classical free condensation solution. Both finite thermal conductivity of the wall and thermocapillary stresses were shown to play an important role, substantially altering the thickness profile.

1. Introduction

Film condensation has been a widely studied topic due to its relevance in many areas of technology. Fundamental understanding of vapor condensation is crucial in a wide variety of thermal management technologies that rely on phase change. A particularly important application is to heat exchangers, where vapor condensation on solid surfaces is often the limiting factor which controls the heat transfer rate.

The first theoretical model of vapor condensation was developed by Nusselt [1] who assumed the thermal resistance is due entirely to the condensate film. Despite this and several other simplifications, Nusselt's theory was found to accurately predict the heat transfer coefficient for free (laminar) condensation of pure vapor on highly conducting surfaces. However, as Othmer discovered later, noncondensables have a tremendous impact on condensation; the presence of as little as 0.5% of air in steam reduces the heat transfer coefficient by half [2]. Othmer's predictions were later confirmed by a number of other studies of steam condensation on vertical flat and cylindrical surfaces [3–7]. The decrease in the heat transfer coefficient is due to the accumulation of noncondensable gas at the vapor-liquid interface, which forms a concentration boundary layer limiting the transport of vapor to the cold surface [8].

There is extensive literature devoted to this subject, with the bulk of theoretical studies focusing on condensation in the presence of forced convection. Forced flows tend to be turbulent, which makes the quantitative description of transport in the gas phase challenging. As a result, theoretical models tend to be rather arbitrary, with dependence on many important parameters expressed in terms of correlations based on empirical data rather than solid fundamental understanding of the problem. In order to make analytical progress, the present study will instead focus on condensation in the presence of free convection.

Given that noncondensable gases tend to dissolve in liquids and are effectively impossible to remove completely, a comprehensive description of the condensation problem and the associated heat transfer has to involve at a minimum the following components. Transport of heat, momentum, and mass should be considered in the gas layer to account for the adverse effect of noncondensables. Transport of both heat and momentum should be considered in the liquid condensate film. Finally, heat transport needs to be considered in the solid wall to account for finite conductivity. The transport equations in the solid, liquid, and gas layer should be solved subject to the appropriate boundary conditions at the solid-liquid and liquid-vapor interface. To our knowledge, only a few studies [9–11] have considered such a comprehensive and self-consistent model, but only numerical analysis has been performed.

* Corresponding author.
E-mail address: liujialj@cqu.edu.cn (J. Liu).

https://doi.org/10.1016/j.ijheatmasstransfer.2018.12.131
0017-9310/

Analytical (and even semi-analytical) results are extremely rare and involve considerable simplification of the problem. One of the most popular approaches, known as the diffusion layer theory, introduced by Peterson and coworkers [12,13] leads to a rather simple, effectively one-dimensional description of transport. The concentration and temperature boundary layers in the gas phase are assumed to be logarithmic, which allows the heat flux to be expressed in terms of the condensation and sensible heat transfer coefficients. Both coefficients, however, are expressed in terms of correlations obtained by previous experimental studies [14], rather than computed from the transport equations. The condensate film is described using a standard lubrication-type model [15], but the corresponding heat transfer coefficient again involves correlations. Despite these rather dramatic simplifications, no explicit solution for the heat transfer coefficient has been obtained, with the resulting system of equations that has to be solved using an iterative procedure. Subsequent studies [6,16,17] used a similar approach.

A considerably more sophisticated and rigorous theoretical description was proposed by Sparrow and Lin [18]. By seeking similarity solutions in the liquid and gas layer, this approach also makes the problem effectively one-dimensional, making it comparable to the diffusion layer theory in terms of complexity. However, the solutions are still constructed iteratively, so no explicit dependence on various parameters can be obtained. Moreover, the validity of this approach crucially relies on the assumption that the solution to the transport equations possess scaling that allows them to be expressed in similarity form. As we argue in the present paper, this assumption becomes invalid when thermocapillary stresses at the liquid-vapor interface are taken into account. Subsequent developments of this approach by Minkowycz and Sparrow [19], Rose [20], and Wu et al. [21] suffer from the same limitations.

While it is widely accepted that thermocapillary stresses play an important role in evaporation, e.g., leading to dry-out in heat pipes [22], oddly enough, the thermocapillary effect is almost universally ignored, without much justification, in considering filmwise condensation. As the present paper demonstrates, thermocapillary stresses arise inevitably in condensate films in response to variation in their thickness and can have a profound effect on the thickness profile and therefore the thermal resistance of the liquid layer. This is a good illustration of the kinds of limitations the lack of an explicit analytical solution describing film condensation can have: in the absence of an expression for the interfacial temperature it is difficult to judge the importance of a physical effect such as thermocapillarity.

The lack of an explicit relation between the heat transfer coefficient and the various material parameters and problem geometry is a significant limitation for our ability to improve thermal management technologies relying on phase change. Our study fills this void by formulating and solving a model describing transport in all three layers (solid/liquid/gas) and provides a clear physical insight into the problem of filmwise condensation in the entire range of the concentration of noncondensables. The focus on free filmwise condensation on a vertical plane allows us to obtain a tractable description that yields an explicit analytical expression for the heat transport coefficient which clearly identifies the physical effects that become the bottleneck in the heat transfer in various limiting cases. Our description also gives an explicit expression for the condensate film thickness profile and, in particular, shows that thermocapillary stresses make it more uniform compared with the boundary layer-type solutions of Nusselt [1] and Sparrow and Lin [18] that have become textbook examples.

The paper is organized as follows. Section 2 describes the mathematical model of the problem. The analysis of the model is presented in Section 3 and some applications in Section 4. Section 6 contains the summary and conclusions.

2. Mathematical model

The problem under consideration involves a mixture of vapor and air in a cavity of length L and height H in the presence of a horizontal temperature gradient. The hot vapor, which is assumed to be saturated on the right side of the cavity, condenses on a cooled vertical wall of thickness h_w on the left side of the cavity, forming a film of thickness h_l, which drains under the action of gravity. The schematic illustration of the respective geometry is shown in Fig. 1. For simplicity we will consider a two-dimensional problem, where all physical observables depend only on the horizontal coordinate x and vertical coordinate z, but not the coordinate y, and the velocity field is planar, $\mathbf{u} = \hat{\mathbf{x}}u + \hat{\mathbf{z}}w$.

2.1. Governing equations

The heat and mass transport in the gas and the liquid condensate film are governed by the mass, momentum, and heat conservation equations

$$\nabla \cdot \mathbf{u}_\iota = 0, \tag{1}$$

$$\rho_\iota(\partial_t \mathbf{u}_\iota + \mathbf{u}_\iota \cdot \nabla \mathbf{u}_\iota) = -\nabla p_\iota + \mu_\iota \nabla^2 \mathbf{u}_\iota + \rho_\iota \mathbf{g}, \tag{2}$$

$$\partial_t T_\iota + \mathbf{u}_\iota \cdot \nabla T_\iota = \alpha_\iota \nabla^2 T_\iota, \tag{3}$$

where p and T are the pressure and temperature, respectively. The mass density ρ, thermal diffusivity α, and dynamic viscosity of the two fluids are considered constant. The index $\iota = g, l$ denotes the gas and the liquid phase, respectively. Finally, mass transport in the gas, which is a binary mixture of vapor and air, is governed by the advection-diffusion equation

$$\partial_t c_v + \mathbf{u}_\iota \cdot \nabla c_v = D \nabla^2 c_v. \tag{4}$$

where c_a and c_v are the molar fractions of air and vapor, respectively, and D is the binary diffusion coefficient. To account for the finite thickness and conductivity of the solid walls, we will also use the heat equation

$$\partial_t T_w = \alpha_w \nabla^2 T_w, \tag{5}$$

where T_w is the temperature of the wall. Thermal diffusivities α_ι are related to thermal conductances k_ι via $k_\iota = \alpha_\iota \rho_\iota C_{p,\iota}$, where $C_{p,\iota}$ is the heat capacity of the gas/liquid/wall ($\iota = g, l, w$).

Since we are interested in the heat transport in steady state, we will set the temporal partial derivatives to zero in all of the above equations. In particular, the steady mass transport Eq. (4) in the gas can be rewritten in the form

$$\nabla \cdot \mathbf{j}_\iota = 0, \tag{6}$$

where

$$\mathbf{j}_\iota = n_g(\mathbf{u}_g c_\iota - D \nabla c_\iota) \tag{7}$$

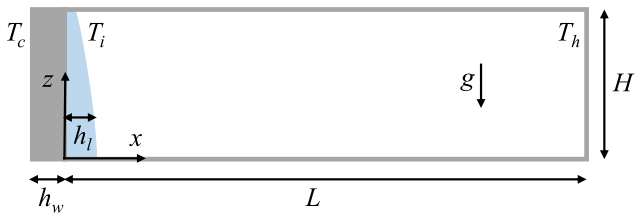

Fig. 1. The geometry of the problem. The mixture of vapor and air (white) is confined inside a cavity of interior dimensions $L \times H$. The cold wall of the cavity (dark gray) is covered by the liquid condensate film (light blue). Gravity points in the negative z direction. (For interpretation of the references to colour in this figure legend, the reader is referred to the web version of this article.)

is the number density flux of component ι, $n_g = n_a + n_v$ is the net number density of the gas, and we have ignored the spatial variation in n_g associated with its dependence on the temperature, such that the molar fraction determines both the partial pressures and the number densities of the two components:

$$c_\iota = \frac{p_\iota}{p_g} = \frac{n_\iota}{n_g}. \tag{8}$$

2.2. Boundary conditions

We will assume there is no heat or mass flux through the top and bottom of the cavity, and on the outer side $x = -h_w$ of the cooled wall the temperature is fixed

$$T_w = T_c, \tag{9}$$

e.g., due to the wall being in contact with a coolant at temperature T_c. We will also assume that on the hot side of the cavity (at $x = L$) the gas has a fixed temperature

$$T_g = T_h \tag{10}$$

and the vapor is saturated. Such boundary conditions would describe a variety of practically relevant situations, e.g., the hot saturated vapor produced by evaporation of the liquid percolating through a porous wall of constant temperature T_h in the geometry shown in Fig. 1 or being injected from an external cavity along the centerline of a channel of width $2L$. The inner side $x = 0$ of the cooled wall is assumed to be covered by a thin layer of liquid condensate of thickness $h_l \ll h_w$. The heat flux balance at this interface requires

$$\mathbf{n} \cdot k_w \nabla T_w = \mathbf{n} \cdot k_l \nabla T_l, \tag{11}$$

where $\mathbf{n} = \hat{\mathbf{x}}$ is the surface normal. The heat flux balance at the liquid-vapor interface $x = h_l$ requires

$$\mathcal{L} J = \mathbf{n} \cdot k_g \nabla T_g - \mathbf{n} \cdot k_l \nabla T_l \tag{12}$$

where $\mathbf{n} = \hat{\mathbf{x}}$ again (since h_l is small), $\mathcal{L}$ is the latent heat of vaporization, and J is the mass flux associated with phase change (here, condensation). The temperature at the liquid-solid and liquid-vapor interfaces is continuous

$$\begin{aligned} T_w &= T_l, \quad x = 0, \\ T_l &= T_g, \quad x = h_l. \end{aligned} \tag{13}$$

The mass/number conservation for the two components of the gas mixture at the liquid-vapor interface requires

$$\begin{aligned} \tfrac{J}{m_v} &= \mathbf{j}_v \cdot \mathbf{n} = n_g(\mathbf{n} \cdot \mathbf{u}_g c_v - D\mathbf{n} \cdot \nabla c_v), \\ 0 &= \mathbf{j}_a \cdot \mathbf{n} = n_g(\mathbf{n} \cdot \mathbf{u}_g c_a - D\mathbf{n} \cdot \nabla c_a), \end{aligned} \tag{14}$$

where m_v is the mass of one vapor molecule. Adding these we can find the normal components of the gas velocity

$$\mathbf{n} \cdot \mathbf{u}_g = \frac{J}{n_g m_v}, \tag{15}$$

and the liquid velocity

$$\mathbf{n} \cdot \mathbf{u}_l = \frac{J}{\rho_l}. \tag{16}$$

According to the kinetic theory of gases [23],

$$J = \beta u_t \rho_v \left[\frac{\sigma\kappa}{\rho_l R_v T_i} + \frac{\mathcal{L}}{R_v}\left(\frac{1}{T_s} - \frac{1}{T_i}\right)\right]. \tag{17}$$

Here R_v is the specific gas constant for the vapor, $u_t = \sqrt{R_v T_i}$ is the characteristic thermal velocity of the gas molecules, $\rho_v = m_v c_v n_g$ is the vapor concentration at the interface, σ is the surface tension, subscripts i and s denote values of the temperature at the interface and the saturation value for the vapor, respectively, and we have defined a shorthand

$$\beta = \sqrt{\frac{1}{2\pi}} \frac{\lambda}{2 - \lambda}, \tag{18}$$

where λ is the accommodation coefficient (which can typically be set to unity). The first term in (17) can be neglected due to the low curvature κ of the liquid-vapor interface. The pressure dependence of the saturation temperature can be expressed using the Clausius-Clapeyron equation

$$\ln \frac{p_v}{p_v^0} = \frac{\mathcal{L}}{R_v}\left[\frac{1}{T_0} - \frac{1}{T_s}\right], \tag{19}$$

where p_v^0 is the saturation pressure at the reference temperature T_0, which we will set equal to T_h.

Finally, the stress balance at the liquid-vapor interface gives

$$(\Sigma_l - \Sigma_g) \cdot \mathbf{n} = \mathbf{n}(\kappa\sigma - J^2/\rho_g) - \gamma \nabla_s T_i \tag{20}$$

where $\Sigma_\iota = \mu_\iota[\nabla \mathbf{u}_\iota + (\nabla \mathbf{u})_\iota^T] - p_\iota$ is the stress tensor, $\nabla_s = (1\text{-}\mathbf{n} \cdot \mathbf{n})\nabla$is the surface gradient, the term J^2/ρ_g describes vapor recoil, $\gamma = -\partial\sigma/\partial T > 0$ is the temperature coefficient of surface tension, and the first term on the right-hand-side can be ignored due to low curvature of the interface. In addition, the tangential velocity components are continuous at $x = h_l$

$$(1 - \mathbf{n} \cdot \mathbf{n})(\mathbf{u}_l - \mathbf{u}_g) = 0 \tag{21}$$

and satisfy the no-slip boundary conditions at the wall ($x = 0$)

$$\mathbf{u}_l = 0. \tag{22}$$

Given that h_l is negligibly small compared with L, in the boundary conditions describing the liquid-vapor interface the quantities describing the gas phase can be evaluated at $x = 0$ instead of $x = h_l$.

3. Analysis

We will start our analysis by considering transport of heat, mass, and momentum in the gas layer, which tends to control the condensation rate and the associated heat transfer coefficient when the fraction of noncondensables exceeds a few percent. We will then consider the conjugate heat transfer problem which involves the gas layer, the condensate film, and the cold wall, where spatial nonuniformity of the condensate film is neglected. Next, we will use the results for the condensation rate to derive a solution for the condensate film thickness that takes into account the gravitational draining as well as the thermocapillary stresses arising due to the nonuniformity of the film. Finally, we will validate the assumptions made in the analysis and illustrate how the results are affected by the concentration of noncondensables using a couple of specific examples.

3.1. Gas layer

It is natural to expect that convective flow in the gas layer could strongly modify the transport of heat and mass towards the cold wall, which would require the flow field to be computed. However, this is not necessarily the case, at least for free convection in cavities with moderate to high aspect ratio $\Gamma = L/H$. As numerical simulations reported in Ref. [24] illustrate, mass transport in the gas phase is often essentially one-dimensional even in the presence of convective flow. This can be understood via a simple calculation focusing on the central region of the cell, which controls the mass transport in the gas phase. Let us introduce the nondimensional coordinates $\chi = x/H$ and $\zeta = z/H$, such that the interior of

the cavity corresponds to $0 < \zeta < 1$ and $0 < \chi < \Gamma$. Since the flow field is constrained to the $\chi - \zeta$ plane and is incompressible, it can be written in terms of the stream function $\psi(\chi, \zeta)$,

$$\mathbf{u}_g = \hat{\mathbf{x}} u_g + \hat{\mathbf{z}} w_g = \hat{\mathbf{x}} \partial_\zeta \psi - \hat{\mathbf{z}} \partial_\chi \psi. \tag{23}$$

In the limit of large Γ, the flow is essentially horizontal in the central region of the cavity with $u_g = O(\bar{u}_g)$ and $w_g = O(\Gamma^{-1}\bar{u}_g)$, where $\bar{u}_g$ is a characteristic flow velocity in the gas layer. We can therefore simplify (4) to read

$$H u_g \partial_\zeta c_v = D(\partial_\chi^2 c_v + \partial_\zeta^2 c_v), \tag{24}$$

with the vertical component u_z of the velocity yielding a higher order (in Γ^{-1}) correction. Furthermore, let $u_g = u_m + u_r$, where $u_m = \text{const} < 0$ is the mean component of the flow (the net flow is towards the cold wall) and u_r describes the recirculation component with zero mean

$$\int_0^1 u_r d\zeta = 0. \tag{25}$$

Correspondingly, we can write $\psi = u_m \zeta + \tilde{\psi}(\zeta) + O(\Gamma^{-1})$, where $u_r = \partial_\zeta \tilde{\psi}$, and

$$\int_0^1 \tilde{\psi}' d\zeta = \tilde{\psi}(1) - \tilde{\psi}(0) = 0. \tag{26}$$

In Ref. [24] the following solution to (24) subject to no-flux boundary conditions at the top/bottom of the gas layer was derived in the special case $u_r = 0$:

$$c_v = C_0 + C_1 e^{-Pe_m \chi}, \tag{27}$$

where $Pe_m = |u_m| H/D$ is the Péclet number, which corresponds to the mean flow and the constants C_0 and C_1 are determined by the boundary conditions at $\chi = 0$ and $\chi = \Gamma$. In the general case (i.e., $u_r \neq 0$) the corresponding solution to (24) is

$$c_v = C_0 + C_1 e^{-Pe_m \chi}[1 + f(\zeta)], \tag{28}$$

where

$$f''(\zeta) = \frac{u_m u_r(\zeta) H^2}{D^2}[1 + f(\zeta)]. \tag{29}$$

The right-hand-side of (29), and hence $f(\zeta)$ itself, is of order $\epsilon = Pe_m Pe_r$, where $Pe_r = \max_z |u_r(z)| H/D$ is the Péclet number describing the strength of the recirculation flow u_r. Specifically,

$$f(\zeta) = \frac{u_m H^2}{D^2} \int \tilde{\psi}(\zeta) d\zeta + O(\epsilon^2). \tag{30}$$

Now, finally, the reason for separating u_x into the two components u_m and u_r becomes clear: the no-flux boundary condition for c_v requires $f'(0) = f'(1) = 0$ which is only consistent with (30) when (26) is satisfied.

It can be shown rigorously that $\epsilon \propto \Delta T^2$, so $\epsilon \ll 1$ for sufficiently small ΔT and any $\bar{c}_a$. Since ϵ is small, the z-dependence of the concentration field is weak, such that (28) reduces to (27) and we can effectively treat c_v as a function of x alone. The accuracy of the analytical solution (27) even for moderate ΔT is also supported by numerical results [24]. Furthermore, since α_g and D are of similar magnitude for gases, the governing Eqs. (3) and (4) are formally equivalent, and so are the boundary conditions for c_v and T_g, the same arguments apply to the temperature field T_g, such that

$$T_g = B_0 + B_1 e^{-Pe_t \chi} + O(\epsilon), \tag{31}$$

where $Pe_t = |u_m| H/\alpha_g$ is the thermal Péclet number and B_0, B_1 are some constants. Since both c_v and T_g can be considered effectively z-independent and the condensate film is essentially flat, we can find solutions for $\mathbf{u}_g, T_l$, and T_w that are also effectively z-independent. The Navier-Stokes Eq. (2) and the incompressibility condition (1) admit the solution

$$\mathbf{u}_g = u_m \hat{\mathbf{x}} + O(\Gamma^{-1}), \tag{32}$$

$$p_g = p_g^0 - \rho_g g z + O(\mu_g u_r / H^2) \approx p_g^0, \tag{33}$$

where

$$p_g^0 = \frac{p_v^0}{c_v|_{x=L}}. \tag{34}$$

The hydrostatic pressure term $\rho_g g z$ is negligible due to the low mass density of the gas and the viscous term $O(\mu_g u_r/H^2)$ is negligible due to the low velocity of the gas. Plugging (32) together with (27) into (14) yields (to leading order in ϵ)

$$\begin{aligned} c_a &= C e^{u_m x/D} = C e^{-rx/L}, \\ c_v &= 1 - C e^{u_m x/D} = 1 - C e^{-rx/L}, \end{aligned} \tag{35}$$

where we have defined a nondimensional parameter

$$r = -\frac{u_m L}{D} = Pe_m \Gamma > 0,$$

which quantifies the mass flux in the gas phase and

$$u_m = \frac{J}{m_v n_g} \tag{37}$$

according to (15). The coefficient C can be related to the average air concentration by integrating (35) over the cavity:

$$C = \frac{\bar{c}_a r}{1 - e^{-r}}. \tag{38}$$

Note that both the diffusion constant

$$D = \frac{p_0}{p_g} D_0 \tag{39}$$

and the total number density

$$n_g = \frac{p_g}{m_v u_t^2} \tag{40}$$

depend on $\bar{c}_a$ through p_g (cf. Eq. (34)). Here we set T_i equal to T_h in evaluating the thermal velocity u_t and D_0 and p_0 refer to the values of the diffusion coefficient and pressure at standard atmospheric conditions. However, since the product $n_g D$ is independent of p_g, the dimensional mass flux

$$J = -\frac{m_v n_g D}{L} r = -J_0 r \tag{41}$$

can only depend on $\bar{c}_a$ through r, where

$$J_0 = \frac{D_0 p_0}{L u_t^2} \tag{42}$$

is a constant (with units of mass flux).

Correspondingly, Eqs. (3) and (5) governing heat transport in the condensate film and the wall reduce to

$$\partial_x^2 T_l = \partial_x^2 T_w = 0 \tag{43}$$

with solutions

$$\begin{aligned} T_w &= T_c + B_w(x + h_w), \\ T_l &= T_i + B_l(x - h_l), \end{aligned} \tag{44}$$

with some constants B_w and B_l. Using the boundary conditions (9)–(13) we obtain

$$T_g = T_h - B\left(e^{u_m x/\alpha_g} - e^{u_m L/\alpha_g}\right) = T_h - B\left(e^{-\eta r x/L} - e^{-\eta r}\right), \tag{45}$$

where $\eta = D/\alpha_g$ is the inverse of the Lewis number (which is independent of p_g and hence $\bar{c}_a$) and

$$B = \frac{\Delta T - \mathcal{L}J_0(Z_l + Z_w)r}{\eta r Z_g^{-1}(Z_l + Z_w) + 1 - e^{-\eta r}}. \tag{46}$$

Here $\Delta T = T_h - T_c$ and $Z_w = h_w/k_w, Z_l = \bar{h}_l/k_l$, and $Z_g = L/k_g$ are the familiar expressions for thermal resistivity of the cold wall, liquid condensate film, and the gas layer, respectively. The thickness h_l of the condensate film (to be discussed later) is nonuniform, hence Z_l is defined in terms of mean thickness $\bar{h}_l$ for now.

3.2. Mass flux

Let us compute the mass flux next. According to (33)–(35) and (45), at the liquid-vapor interface

$$\begin{aligned} T_i &= T_g|_{x=0} = T_h - B(1 - e^{-\eta r}), \\ \rho_v &= m_v n_g c_v|_{x=0} = \tfrac{1-\bar{c}_a r - e^{-r}}{1-e^{-r}} m_v n_g, \\ p_g &= \tfrac{p_v^0}{c_v|_{x=L}} = \tfrac{1-e^{-r}}{1-(1+r\bar{c}_a)e^{-r}} p_v^0. \end{aligned} \tag{47}$$

Since $p_v = c_v p_g$, the saturation temperature T_s can be computed from (19) by evaluating the vapor concentration at the interface, yielding

$$\frac{1}{T_s} = \frac{1}{T_h} - \frac{R_v}{\mathcal{L}} \ln\left(\frac{c_v|_{x=0}}{c_v|_{x=L}}\right) = \frac{1}{T_h} - \frac{R_v}{\mathcal{L}} \ln\left(\frac{\bar{c}_a r + e^{-r} - 1}{\bar{c}_a r e^{-r} + e^{-r} - 1}\right). \tag{48}$$

Finally, the nondimensional flux r can be computed by substituting (41) and (48) into (17), which yields

$$\begin{aligned} r = &-\frac{\beta \mathcal{L} u_t L}{R_v D} \frac{1 - \bar{c}_a r - e^{-r}}{1 - e^{-r}} \\ &\times \left[\frac{1}{T_h} - \frac{1}{T_h - B(1 - e^{-\eta r})} - \frac{R_v}{\mathcal{L}} \ln\left(\frac{1 - \bar{c}_a r - e^{-r}}{1 - \bar{c}_a r e^{-r} - e^{-r}}\right)\right], \end{aligned} \tag{49}$$

where B and D depend on r and/or $\bar{c}_a$ according to (46) and (39).

An exact solution to the transcendental Eq. (49) cannot be obtained analytically. However, a reasonably accurate approximate solution can be obtained in explicit form by linearizing this equation about $r = 0$ and $\Delta T = 0$:

$$r = \Delta T \left[\frac{D_0 p_0 \mathcal{L} Z_2}{u_t^2 L} + \frac{D_0 p_0 T_h k_g u_t Z_3}{\beta \mathcal{L} L^2 p_v^0} + \frac{\bar{c}_a T_h k_g u_t^2 Z_3}{(1 - \bar{c}_a)\mathcal{L} L}\right]^{-1}, \tag{50}$$

where

$$Z_2 = Z_w + Z_l \tag{51}$$

is the thermal resistance of the wall and the condensate film and

$$Z_3 = Z_w + Z_l + Z_g \tag{52}$$

is the thermal resistance of the wall, the condensate, and the gas layer. We can rewrite (50) in nondimensional form

$$r = \frac{u_t^2 L \Delta T}{D_0 p_0 \mathcal{L} Z}, \tag{53}$$

or, using (41), in dimensional form

$$J = -\frac{\Delta T}{\mathcal{L} Z}, \tag{54}$$

where the net thermal resistance

$$Z = Z_2 + \frac{Z_3}{Z_g}(Z_i + Z_d) \tag{55}$$

includes the contributions describing the interfacial resistance

$$Z_i = \frac{T_c u_t^3}{\beta \mathcal{L}^2 p_v^0} \tag{56}$$

and the diffusive resistance of the gas layer

$$Z_d = \frac{\bar{c}_a}{1 - \bar{c}_a} \frac{L T_c u_t^4}{D_0 p_0 \mathcal{L}^2}. \tag{57}$$

The last expression corresponds to the effective condensation thermal conductivity

$$k_c = \frac{1 - \bar{c}_a}{\bar{c}_a} \frac{D_0 p_0 \mathcal{L}^2}{T_c u_t^4} = \frac{L}{Z_d} \tag{58}$$

derived by Peterson et al. [12].

It is worth emphasizing that, under the most general conditions, the net thermal resistance is not given by a simple sum of the resistances of the wall condensate film, interfacial resistance, and diffusive resistance, but also depends on the thermal resistance of the gas layer in a nontrivial way. However, under typical conditions, due to both the large thickness of the gas layer and its poor thermal conductivity, Z_g will be many orders of magnitude larger than $Z_l + Z_w$ for any $\bar{c}_a$, so that (55) can be simplified:

$$Z \approx Z_w + Z_l + Z_i + Z_d. \tag{59}$$

The corresponding net heat flux is the sum of the latent and sensible heat contributions

$$Q = -\mathcal{L}J + k_g \partial_x T_g|_{x=0}, \tag{60}$$

so that the corresponding heat transfer coefficient is given by

$$\mathcal{H} = \frac{Q}{\Delta T} = \frac{1}{Z_3} + \frac{Z_g}{Z_3}\frac{1}{Z}. \tag{61}$$

It can be further simplified when $Z_3 \approx Z_g \gg Z$, in which case

$$\mathcal{H} \approx \frac{1}{Z}. \tag{62}$$

This result can also be derived from (54) and gives the expression for the heat transfer coefficient in a simple analytical form which (i) includes dependence on the problem geometry and material parameters and (ii) is easy to interpret. Specifically, we find that $\mathcal{H}$ is simplify the inverse of the net thermal resistance, which is a sum of four contributions: the resistance of the cooled wall and the liquid condensate film, interfacial resistance, and the diffusive resistance of the gas layer.

3.3. Condensate film

Up until now we have assumed that the condensate film thickness h_l is small and the variation in the thermal resistance Z_l is negligible. We need to check whether this is indeed the case. The flow inside this thin film can be described using lubrication approximation, where $\mathbf{u}_l = w_l(x)\hat{\mathbf{z}}$. In this approximation, the pressure in the liquid can be computed using (20)

$$p_l = p_g^0 - \rho_g g z - \sigma\kappa, \tag{63}$$

where the curvature of the interface is $\kappa = \partial_z^2 h_l$ and we have ignored the small vapor recoil pressure term. The vertical component of the Navier-Stokes Eq. (2) therefore reduces to

$$\mu_l \partial_x^2 w_l = \rho_l g + \partial_z p_l \approx \rho_l g - \sigma \partial_z^3 h_l, \tag{64}$$

since $\rho_l \gg \rho_v$. The solution satisfying the boundary conditions (20) and (22) is

$$w_l = \frac{\rho_l g - \sigma \partial_z^3 h_l}{2\mu_l}(x^2 - 2h_l x) - \frac{\gamma\tau}{\mu_l} x, \tag{65}$$

where $\tau = \partial_z T_i$ is the interfacial temperature gradient. Under our assumptions, the heat and mass flux are both independent of z, so that

$$Q \approx \frac{\Delta T}{Z} = k_l \frac{T_i - T_{wl}}{h_l}, \tag{66}$$

where T_{wl} is the temperature of the wall-liquid interface that is also independent of z. Hence,

$$\tau = \frac{\partial T_i}{\partial h_l}\partial_z h_l = \frac{\Delta T}{Z k_l}\partial_z h_l. \tag{67}$$

The corresponding volumetric flux is

$$q = \int_0^{h_l} w_l dx = \frac{\sigma h_l^3 \partial_z^3 h_l}{3\mu_l} - \frac{\rho_l g h_l^3}{3\mu_l} - \frac{\gamma \Delta T}{2\mu_l Z k_l} h_l^2 \partial_z h_l. \tag{68}$$

Mass conservation in the liquid together with the mass flux balance (16) requires that

$$\partial_z q = \frac{J}{\rho_l} \approx -\frac{\Delta T}{\rho_l \mathcal{L} Z}, \tag{69}$$

where $q = 0$ at the top of the cell $z = H$ (no flux through the top wall). Integrating this and substituting into (68) yields

$$-\frac{\sigma h_l^3 \partial_z^3 h_l}{3\mu_l} + \frac{\gamma \Delta T}{2\mu_l Z k_l} h_l^2 \partial_z h_l + \frac{\rho_l g h_l^3}{3\mu_l} = \frac{\Delta T}{\rho_l \mathcal{L} Z}(H - z). \tag{70}$$

The terms on the left-hand-side of this equation describe, respectively, the Young-Laplace pressure associated with the curvature of the interface, the thermocapillary stresses, and the gravitational draining, while the term on the right-hand-side describes the condensation mass flux.

The first term in (70) can be neglected if there are no high-curvature regions, such that the resulting differential equation can be rewritten as

$$\delta f' + f = 1 - \zeta, \tag{71}$$

where $f = (h/h_0)^3$, prime denotes the derivative with respect to the nondimensional vertical coordinate ζ,

$$\delta = \frac{\gamma \Delta T}{2 Z k_l H \rho_l g} \tag{72}$$

is a (small) nondimensional parameter which determines the strength of thermocapillary stresses relative to gravity, and

$$h_0 = \left[\frac{3\mu_l H \Delta T}{\rho_l^2 g \mathcal{L} Z}\right]^{1/3} \tag{73}$$

is a characteristic thickness scale which describes the flux balance between condensation and draining due to gravity. Eq. (71) can be solved analytically, yielding

$$h_l = h_0\left(1 - \zeta + \delta\left[1 - A e^{-\zeta/\delta}\right]\right)^{1/3}, \tag{74}$$

where A is some constant. In fact, we should set $A = 0$ to ensure that the solution is well-behaved at $z = 0$ for $\delta \to 0$, which yields the following result for the mean thickness

$$\bar{h}_l = \frac{1}{H}\int_0^H h_l dz = \frac{3}{4} h_0\left[(1+\delta)^{4/3} - \delta^{4/3}\right]. \tag{75}$$

In deriving the solution (74), we assumed that Z is constant. This will not be the case when the overall thermal resistance is dominated by that of the condensate layer. In the (near) absence of air and for a highly conducting cooled wall, $Z \approx Z_l = h_l/k_l$, so neither h_0 nor δ is constant. In this limit, we can rewrite (70) as

$$\frac{\gamma \rho_l \mathcal{L}}{2\mu_l k_l H^2} h_l^2 \partial_\zeta h_l + \frac{\rho_l^2 g \mathcal{L} h_l^4}{4\mu_l k_l H \Delta T} = 1 - \zeta, \tag{76}$$

where we have again dropped the curvature term. An analytical solution for (76) cannot be obtained in the entire interval $0 \leqslant \zeta \leqslant 1$, but it is easy to construct a very piecewise approximation. For $\zeta < 1 - \varepsilon$, where

$$\varepsilon = \left[\frac{\mathcal{L}\gamma^4 \Delta T^3}{64\,\mu_l \rho_l^2 k_l H^5 g^3}\right]^{1/5}, \tag{77}$$

the dominant balance is between the gravitational force and the condensation mass flux, and we recover the classical Nusselt solution (78)

$$h_l = \left[\frac{4\mu_l k_l H \Delta T(1-\zeta)}{\rho_l^2 g \mathcal{L}}\right]^{1/4}. \tag{78}$$

For $\zeta > 1 - \varepsilon$, the dominant balance is between the gravitational force and the thermocapillary stresses. so that

$$h_l = \frac{2\gamma \Delta T}{\rho_l g H(\zeta - \zeta_0)}, \tag{79}$$

where $\zeta_0 < 1 - \varepsilon$ is a constant that can be determined using a matched asymptotic expansion in ε, so long as $\varepsilon \ll 1$ (as we will see below, in practice ε indeed tends to be quite small). In this limit, we can neglect the effect of the deviation of the film thickness profile from the Nusselt solution near $\zeta = 1$ ($z = H$) on the overall heat and mass flux associated with condensation, yielding the mean heat flux

$$Q = \int_0^1 \frac{\mathcal{L}\Delta T k_l}{h_l} d\zeta = \left[\frac{64\rho_l^2 g k_l \mathcal{L}^5}{81\mu_l H}\right]^{1/4} \Delta T^{3/4}. \tag{80}$$

Note that in our model the thickness of the condensate film does not vanish at the top of the cold wall (as illustrated by both (74) and (79)). This should not be very surprising, since the condensate film is in contact with the top wall of the cavity. The curvature of the free surface also remains finite at $\zeta = 1$, instead of blowing up as it does for the Nusselt solution. This is due to thermocapillarity, which suppresses draining, making the condensate slightly thicker and more spatially uniform. The solution(s) we have obtained can be made to accommodate additional boundary conditions at $\zeta = 1$ such as the fixed contact angle with the top wall or the vanishing of the film thickness (e.g., for a perfectly nonwetting wall or in the absence of a top wall), but this requires that the curvature term be included in the lubrication approximation. Since the condensate film is typically very thin, the effect of the film curvature is limited to a region of size $O(h_l)$ near from $z = H$. The deviation of the solution in this region from the form derived here will therefore have a negligible influence on the condensation rate as $h_l \ll H$.

4. Applications

To illustrate these results, we will discuss how they depend on the choice of the coolant fluid, the wall material, and the amount of noncondensable gases present in the cavity, which are among the most accessible design parameters. Following a series of previous numerical [25,26,24], analytical [27], and experimental [28] studies, we will assume that a shallow layer of liquid coolant is confined inside a sealed rectangular cavity (cf. Fig. 2). An external temperature gradient is applied by maintaining the exterior surface of the cold wall at temperature T_c and the exterior of the hot wall at temperature $T_h = T_c + \Delta T$. As in a typical heat pipe, the liquid coolant evaporates at (or near) the hot wall, the vapor flows towards, and condenses, on the cold wall. To simplify things, we will avoid the discussion of evaporation and the temperature drop across the hot wall and simply assume that the hot wall is

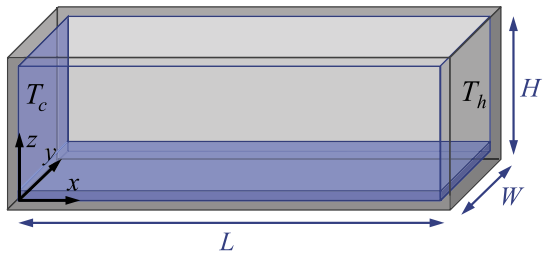

Fig. 2. Test cell containing the liquid and air/vapor mixture. A layer of liquid (light blue) is at the bottom of the cell and a thin film of condensate covers the entire cold wall. Thermal gradient in the x direction is imposed by maintaining the end walls at temperatures T_c and $T_h > T_c$. (For interpretation of the references to colour in this figure legend, the reader is referred to the web version of this article.)

isothermal and the vapor is in thermal equilibrium with the liquid at $x = L$. We will assume that the geometry ($L = 48.5$ mm, $H = 10$ mm, $h_w = 1.25$ mm), reference temperature ($T_c = 293$ K), and the applied temperature differential ($\Delta T = 10$ K) are fixed at the values considered in the studies referenced above.

4.1. Silicone oil condensation on fused quartz

We will start by considering a volatile (0.65 cSt) silicone oil confined inside a test cell made of fused quartz (the values of all material parameters can be found in Ref. [24]). All of our calculations were restricted to a range of $\bar{c}_a$ varying from a minimum of 0.001 (i.e., 0.1% air), which in all likelihood is well below the value that can be achieved in practice, to the maximum $1 - p_v^0/p_0$, which corresponds to the atmospheric pressure p_0, when the gas predominantly contains air ($\bar{c}_a = 0.96$).

In order to obtain solutions, exact or approximate, of the model, we first substitute (59), (72), and (73) into (75) and solve the resulting equation for the mean thickness of the condensate film $\bar{h}_l$ for a fixed $\bar{c}_a$. The results for different $\bar{c}_a$ are plotted in Fig. 3, which shows that $\bar{h}_l$ varies from the maximum of around 35 μm when there is essentially no air inside the cell to around 2.6 μm at ambient conditions, when the gas is predominantly air with only 4% vapor. The thickness profile $h_l(\zeta)$ for the lowest value of the air concentration $\bar{c}_a = 0.001$ is shown in Fig. 4. The thickness of the film varies between 15 μm at the top of the cold wall ($\zeta = 1$) to 46 μm at the bottom ($\zeta = 0$).

Once the thickness of the condensate film has been determined, its thermal resistance can be found, which allows computation of the mass and heat flux associated with the condensation process. The condensation mass flux J (or rather its absolute value, since $J < 0$) and the corresponding heat transfer coefficient $\mathcal{H}$ are shown in Fig. 5. The approximate analytical solution is found to be

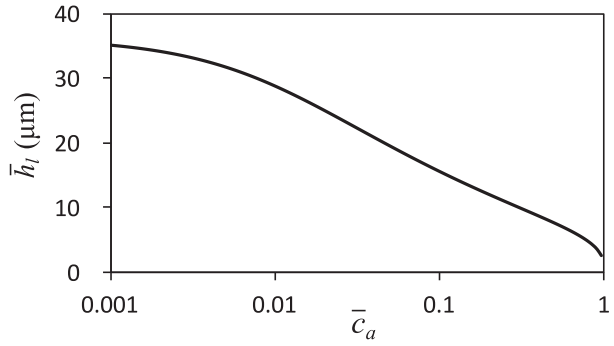

Fig. 3. Dependence of the average thickness $\bar{h}_l$ of the condensate film on the air concentration $\bar{c}_a$ for condensation of silicone oil on fused quartz.

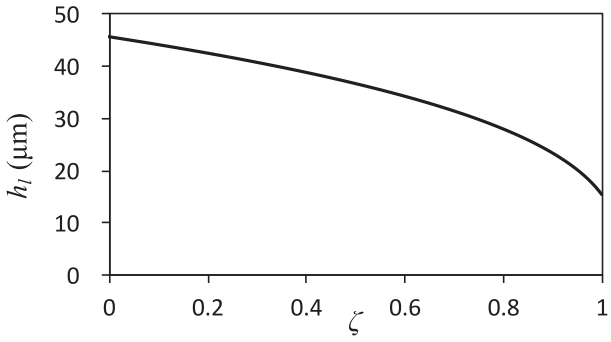

Fig. 4. Thickness profile $h_l(\zeta)$ of the silicone oil condensate film for $\bar{c}_a = 0.001$.

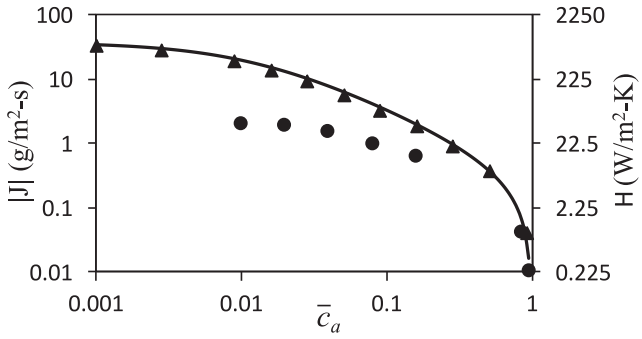

Fig. 5. Dependence of the mass flux J and heat transfer coefficient $\mathcal{H}$ on the air concentration $\bar{c}_a$ for condensation of silicone oil on fused quartz. Exact numerical solution is shown as a solid curve, the approximate analytical solution as triangles, and the numerical result from Ref. [24] as circles.

virtually indistinguishable from the exact numerical solution in the entire range of composition of the gas phase, which attests to the excellent accuracy of the approximation. The figure also compares these results with the numerical ones obtained in a previous study [24] which assumed that the walls of the container are partially wetting, so that condensation occurs exclusively at the surface of the liquid layer which covers the bottom of the cell (cf. Fig. 2). Not surprisingly, the condensation mass flux (and therefore the heat transfer coefficient) is notably higher when the vapor condenses on the cold wall instead. The difference can be as large as an order of magnitude at low values of $\bar{c}_a$ under otherwise identical conditions and reflects both the larger area over which the condensation occurs and the smaller thermal resistance of the thin film of condensate covering the cold wall.

In conclusion of this section, let us compare the magnitudes of the different contributions to the overall thermal resistance Z of

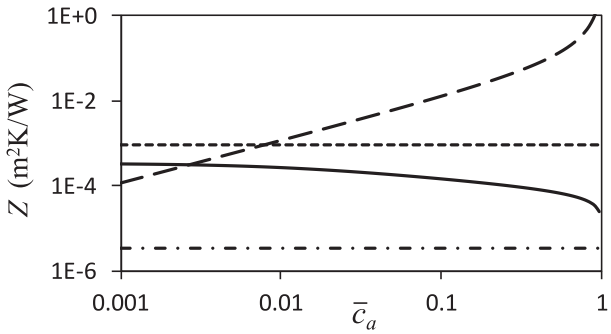

Fig. 6. Thermal resistance of the condensate film (Z_l, solid line), the wall (Z_w, short-dash line), the interfacial resistance (Z_i, dash-dot line), and the diffusive resistance of the gas layer (Z_d, long-dash line) for silicone oil condensation on fused quartz as a function of air concentration.

the system. The four contributions (Z_d, Z_i, Z_l, and Z_w) are plotted as a function of the average concentration of air $\bar{c}_a$ in Fig. 6. Not surprisingly, at high $\bar{c}_a$ when mass transport is strongly suppressed by diffusion through air, thermal resistance is dominated by the diffusive contribution. In fact Z_d remains the largest contribution even when the gas contains as little as 1% of air. At even smaller air concentrations, the thermal resistance of the wall becomes the dominant contribution, which is also not surprising given that the walls are relatively thick and fused quartz is a relatively poor conductor. The thermal resistance of the condensate film and the interfacial resistance are negligible in this particular scenario, but may become important when the wall material has high thermal conductivity, as illustrated in the next chapter.

4.2. Water condensation on copper

A more practical application of our study is towards characterizing heat transfer in heat pipes and heat spreaders, which commonly use water as the coolant inside sealed copper containers. Hence, we will next consider water confined inside a test cell made of copper, but with the geometry (length, height of the cavity, wall thickness) that is the same as that considered in the previous section to enable direct comparison.

The average thickness $\bar{h}_l$ of the condensate film is plotted as a function of $\bar{c}_a$ in Fig. 7. It varies from the maximum of around 44 μm at $\bar{c}_a = 0.001$ to around 2 μm at ambient conditions, when the gas mixture contains just over 2% of water vapor. This is very similar to the results we have obtained for silicone oil, since, for the water/copper combination, the higher latent heat is offset by the lower overall thermal resistance in the denominator of (73). The thickness profile $h_l(\zeta)$ for the lowest value of the air concentration $\bar{c}_a = 0.001$ is shown in Fig. 8. The thickness of the condensate film varies between 27 μm at the top of the cold wall ($\zeta = 1$) to 54 μm at the bottom ($\zeta = 0$), also similar to the result of the previous section.

The corresponding condensation mass flux J and heat transfer coefficient $\mathcal{H}$ are shown in Fig. 9. Again we find the approximate analytical solution to be in good agreement with the exact numerical solution in the entire range of composition of the gas phase. The agreement can be improved further by keeping higher-order terms in the expansion of (50). The condensation mass flux is comparable to that for the silicone oil/fused quartz case (as in the case of condensate film thickness, this is because for the water/copper combination the higher latent heat is offset by the lower overall thermal resistance in the denominator of (69)). In contrast, the heat transfer coefficient is substantially higher for the water/copper combination: for $\bar{c}_a = 0.001$ we find $\mathcal{H} \approx 10^4$ W/(m^{2}K) compared with $\mathcal{H} \approx 750$ W/(m^{2}K) for the silicone oil/fused quartz

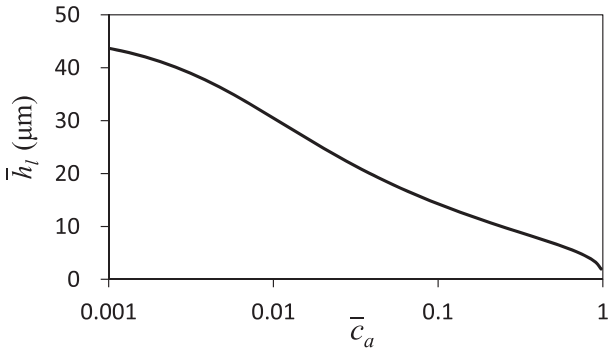

Fig. 7. Dependence of the average thickness $\bar{h}_l$ of the condensate film on the air concentration $\bar{c}_a$ for condensation of water on copper.

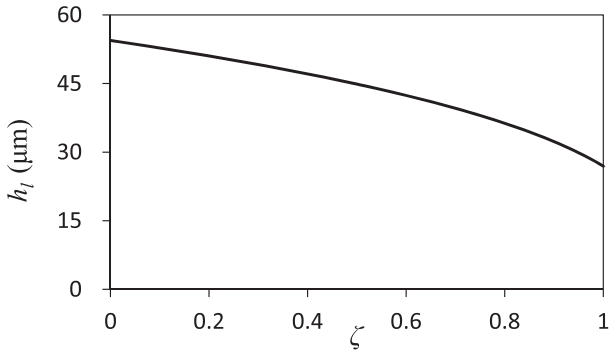

Fig. 8. Thickness profile $h_l(\zeta)$ of the water condensate film for $\bar{c}_a = 0.001$.

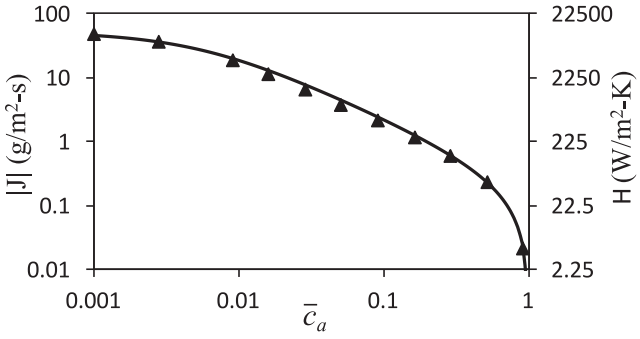

Fig. 9. Dependence of the mass flux J and heat transfer coefficient $\mathcal{H}$ on the air concentration $\bar{c}_a$ for condensation of water on copper. Exact numerical solution is shown as a solid curve and the approximate analytical solution as triangles.

combination, illustrating the clear advantage of water (due to its high latent heat) and copper (due to its high thermal conductivity).

The magnitudes of the different contributions to the overall thermal resistance Z are compared in Fig. 10. We find that thermal resistance is dominated by the diffusive contribution over almost the entire range of $\bar{c}_a$. Thermal resistance of the condensate film becomes the dominant contribution only at extremely low $\bar{c}_a$ when the gas contains merely 0.3% of air, which in all likelihood is impossible to achieve in practice, since air tends to dissolve reasonably well in water. As expected, thermal resistance of the wall is negligible because copper is a very good thermal conductor. Similarly, the interfacial resistance (56) is negligibly small due to the high latent heat of water.

As the two examples considered here illustrate, the thermal resistance of the condensate film becomes the dominant factor

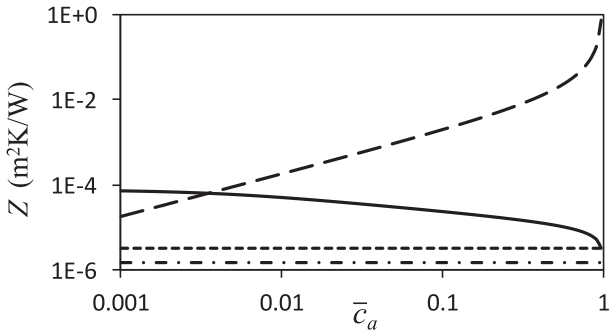

Fig. 10. Thermal resistance of the condensate film (Z_l, solid line), the wall (Z_w, short-dash line), the interfacial resistance (Z_i, dash-dot line), and the diffusive resistance of the gas layer (Z_d, long-dash line) for water condensation on copper as a function of air concentration.

limiting heat and mass flux only under rather extreme conditions (when noncondensables have been effectively completely removed) that may never be realized in practice. It is only in this case that the one-dimensional approximation for the heat and mass transport in the gas phase may become invalid. However, even in this limit our model should produce reasonably accurate predictions for the net heat and mass flux. Note that the condensate film thickness profile in this limit (cf. Figs. 4 and 8) remains relatively uniform, unlike the unphysical Nusselt's solution which predicts that the condensate film thickness vanishes at the top of the cold wall, resulting in a divergence of the heat and mass flux there. Our results predict no divergence, with the film thickness h_l and therefore its local thermal resistance h_l/k_l varying relatively little about the mean. As a result, heat and mass flux in the gas layer, especially at high aspect ratio Γ can be still be considered effectively one-dimensional.

Finally, let us comment on the effect of geometry on the condensate film thickness. As Eqs. (73) and (75) illustrate, $\bar{h}_l \propto H^{1/3}$ for all $\bar{c}_a$. The dependence on the thickness L of the gas layer is due primarily to the diffusive resistance (57), which becomes dominant at typical conditions when the gas contains more than about 0.3% air, when $\bar{h}_l \propto (H/L)^{1/3} = \Gamma^{-1/3}$. This scaling illustrates how weak the predicted dependence of $\bar{h}_l$ (and hence Z_l) on the geometry is.

5. Comparison with experimental data

Direct quantitative comparison of the predictions of our model with experiment is significantly complicated by a number of factors. Consider, for instance, the composition of the gas, which is the most important factor controlling condensation rate at typical conditions achievable in practice, i.e., when the fraction of noncondensables is not vanishingly small and $Z \approx Z_d$. In our model it is described using the spatial average $\bar{c}_a$ over the entire volume of the gas phase. However, this average is only meaningful for a fixed geometry, e.g., distance L between the hot wall ("evaporator") and the cold wall ("condenser"). As solution (35) illustrates, the air concentration profile is exponential, with a concentration boundary layer of thickness

$$\delta_a = \frac{L}{r} = \frac{D_0 p_0 \mathcal{L} Z}{u_t^2 \Delta T}, \tag{81}$$

forming next to the cold wall and $c_a \ll 1$ for $x \gg \delta_a$. At sufficiently high condensation rates, δ_a becomes smaller than L and is given by

$$\delta_a \approx \frac{T_c}{\Delta T} \frac{u_t^2}{\mathcal{L}} \int_0^L c_a \, dx \tag{82}$$

and hence

$$Z_d \approx \frac{u_t^2 \Delta T \delta_a}{D_0 p_0 \mathcal{L}} \tag{83}$$

becomes independent of the geometry and determined by the *total amount* of air in the gas phase rather than its *average concentration* reported in most experimental studies. Note that $\bar{c}_a \propto L^{-1}$, so that Z_d can remain finite while $\bar{c}_a \to 0$, e.g., as $L/\delta_a \to \infty$.

We are not aware of any experimental studies that provide a sufficiently detailed description of the experimental apparatus and reliable measurements of the composition in the gas phase required for comparison of the *absolute* values of the mass/heat flux or the heat transfer coefficient at different concentrations of noncondensable gases. Hence, like many previous theoretical studies, we will compare *normalized* heat fluxes

$$Q' = \frac{Q}{Q^*}, \tag{84}$$

as a function of the (average) concentration of air, where Q^* is a fixed reference heat flux chosen appropriately for each experiment (and the model). To minimize the error inherent in any reference measurement, we will compute Q^* using a suitable average over the entire range of concentrations explored in a particular experiment. In the model, according to (57) we can choose Q^* such that

$$Q' = \frac{1 - \bar{c}_a}{\bar{c}_a}. \tag{85}$$

For experimental data, we chose Q^* such that it minimizes the least squares deviation

$$E = \sum_i \left(\frac{1 - \bar{c}_a^i}{\bar{c}_a^i} - \frac{Q^i}{Q^*} \right)^2, \tag{86}$$

where Q^i is the heat flux measured at the average concentration $\bar{c}_a^i$. Fig. 11 compares the predictions of our model with experimental data of Kataoka et al. [29] (for initial air pressure of 0.1 MPa) and Uchida et al. [30] in the limit where Z_d is dominant. As the figure illustrates, the model predictions agree reasonably well with the measurements obtained in the experimental studies.

To get a sense of how the predictions of our model compare with experiment in absolute terms, consider the case of pure vapor, where the uncertainty in the composition of the gas phase is sufficiently small for an apples-to-apples comparison. The experimental measurements of the heat flux at different ΔT by Al-Diwany and Rose [3] and the predictions of our model are shown in Fig. 12. The value of T_h was reported in that study for the heat flux measurements in the presence of noncondensable gases (Argon and Helium), but not for pure vapor. We estimated $T_h = 65$ C, which is similar to the values measured in the presence of noncondensables. Since some material parameters (most notably the viscosity μ_l) vary significantly with temperature, we evaluated all of them at $T_c = T_h - \Delta T$.

We find the agreement to be quite good in the entire range of ΔT, with the discrepancy between theory and experiment being no larger than the uncertainty in the experimental measurements. Perhaps even more unexpected is the fact that the predictions based on the spatially averaged thermal resistance $Z_l = \bar{h}_l/l_l$ corresponding to the solution (74) are almost identical to those based on the Nusselt solution (78), where $Z_l = h_l/k_l$ varies with height. This both validates the assumptions made in deriving our analytical solutions and suggests that our predictions for the condensation rate and heat flux remain accurate when thermal resistance is dominated by the condensate film.

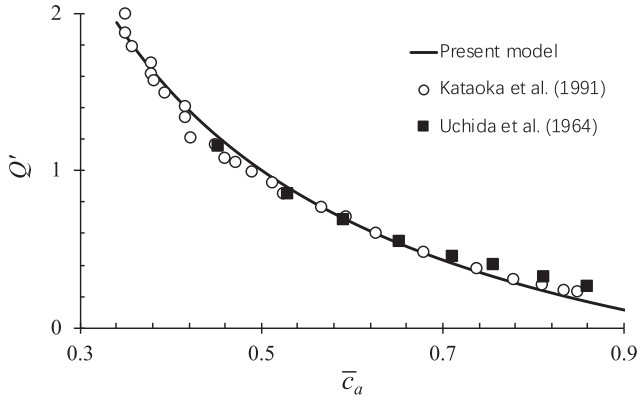

Fig. 11. Normalized heat flux Q' as a function of air concentration $\bar{c}_a$. The predictions of our model are shown as a solid curve and the experimental results as symbols.

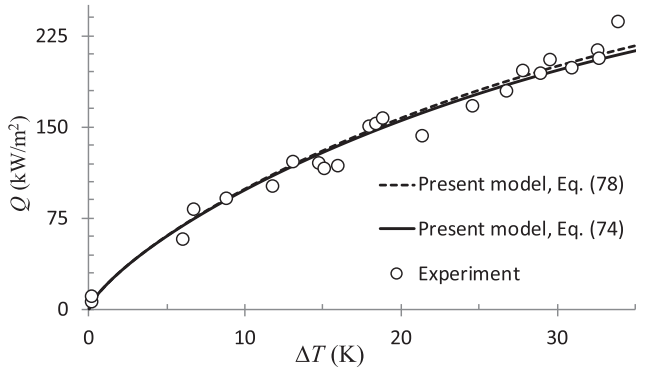

Fig. 12. Comparison of the heat flux Q predicted by our model with the experimental data of Al-Diwany and Rose [3].

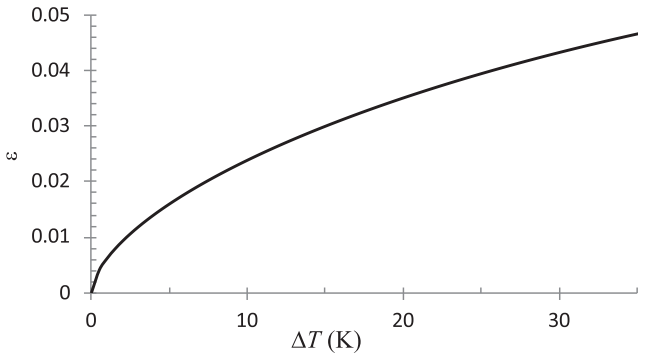

Fig. 13. Nondimensional crossover length scale at which the Nusselt solution (78) breaks down for the geometry considered by Al-Diwany and Rose [3].

In conclusion, Fig. 13 presents the results for the crossover length scale (77) from the top of the film at which the Nusselt solution breaks down. We find that, at the top few percent of the cooled wall, the film thickness is controlled by the balance between thermocapillary stresses and gravitational draining that pull the condensate in the opposite directions. As suggested previously, $\varepsilon \ll 1$ for all ΔT, so the thickness profile in the crossover region $\zeta = O(\varepsilon)$ and the constant ζ_0 in (79) can in principle be found using a perturbation expansion in ε. On the other hand, if one is only interested in the net or average heat or mass flux, the Nusselt solution provides a reasonably good approximation due to the small size of this region.

6. Conclusions

In this paper we have introduced and solved a comprehensive physical model of filmwise vapor condensation under the assumption of free convection. Unlike common engineering models that take a piecemeal approach and treat only a few aspects of the problem, our approach describes all aspects of the problem, including heat and mass transport through the gas phase, interfacial and thermal resistance of the condensate film, and heat conduction through the cooled wall in a self-consistent manner. We have shown that heat and mass transport in the gas layer can be considered one-dimensional under rather general conditions, even when there is convective flow present. Most importantly, we have obtained an approximate analytical solution which shows good agreement with the exact numerical solution of the model in the presence of an arbitrary amount of noncondensable gases such as air.

The analytical solution for the condensation mass flux (and the corresponding heat flux) allows an easy interpretation, with explicit dependence on all of the parameters of the problem. For example, the net thermal resistance is found to be given by a sum of the thermal resistances of the wall, the condensate film, the interfacial resistance, and the diffusive resistance of the gas layer – all given by the familiar standard expressions – in the limit of infinite thermal resistance of the gas layer. This simplicity is, however, misleading. The simple additive expression breaks down when the thermal resistance of the gas layer becomes comparable to the combined thermal resistance of the wall and the condensate film. In the latter case, the more complicated expression (55) has to be used instead. It is worth noting that neither the form of this more general expression, nor the conditions under which the simpler expression breaks down are obvious.

Furthermore, the condensate film thickness profile was derived from first principles using lubrication approximation. Self-consistency of the solution for mass transport across the gas and liquid layer and heat transport through the gas, liquid, and solid layer allowed us to obtain a solution that is different from that predicted by Nusselt's classical free condensation theory [1]. In particular, we have shown that the unavoidable thermocapillary stresses cannot be neglected and play an important role, notably changing the thickness profile, making it flatter. The effect of thermocapillary stresses is especially important near the top of the cold wall, where the thickness of the condensate film remains finite (and as large as 50% of the maximal thickness at the bottom of the cold wall in the geometry considered here). As a result, no unphysical singularities (e.g., in the heat/mass flux) arise in the present description.

One of the assumptions made in this study (the outside temperature of the cooled wall being constant) can be easily relaxed as long as the wall thickness is much less than its height H. For instance, if the heat is removed by the liquid coolant flowing from top to bottom, a vertical temperature gradient will appear on the outside of the wall, which will augment the temperature gradient on the inside due to the variation in the thickness of the condensate film. This will enhance the thermocapillary stresses and can make the film even more uniform.

Conflict of interest

The authors declared that there is no conflict of interest.

Acknowledgments

This work was supported by the National Science Foundation under Grant No. CMMI-1511470. J.L.acknowledges support by National Natural Science Foundation of China (Grant No. 51276203) for sponsoring her visit to Georgia Institute of Technology.

References

[1] W. Nusselt, Die oberflachenkondensation des wasserdampfes, Z. Ver. Dtsch. Ing. 60 (1916) 569.
[2] D.F. Othmer, The condensation of steam, Ind. Eng. Chem. 21 (6) (1929) 576–583.
[3] H. Al-Diwany, J. Rose, Free convection film condensation of steam in the presence of non-condensing gases, Int. J. Heat Mass Transf. 6 (7) (1973) 1359–1369.
[4] S. Park, M. Kim, K. Yoo, Condensation of pure steam and steam-air mixture with surface waves of condensate film on a vertical wall, Int. J. Multiph. Flow 22 (5) (1996) 893–908.
[5] S. Al-Shammari, D. Webb, P. Heggs, Condensation of steam with and without the presence of non-condensable gases in a vertical tube, Desalination 169 (2) (2004) 151–160.
[6] K.-Y. Lee, M.H. Kim, Experimental and empirical study of steam condensation heat transfer with a noncondensable gas in a small-diameter vertical tube, Nucl. Eng. Des. 238 (1) (2008) 207–216.

[7] J. Su, Z. Sun, G. Fan, M. Ding, Experimental study of the effect of non-condensable gases on steam condensation over a vertical tube external surface, Nucl. Eng. Des. 262 (2013) 201–208.
[8] A.P. Colburn, O.A. Hougen, Design of cooler condensers for mixtures of vapors with noncondensing gases, Indust. Eng. Chem. 26 (11) (1934) 1178–1182.
[9] M. Saraireh, G. Thorpe, et al., Condensation of vapor in the presence of non-condensable gas in condensers, Int. J. Heat Mass Transf. 54 (17-18) (2011) 4078–4089.
[10] C. Chantana, S. Kumar, Experimental and theoretical investigation of air-steam condensation in a vertical tube at low inlet steam fractions, Appl. Therm. Eng. 54 (2) (2013) 399–412.
[11] C. Zhang, P. Cheng, W. Minkowycz, Lattice boltzmann simulation of forced condensation flow on a horizontal cold surface in the presence of a non-condensable gas, Int. J. Heat Mass Transf. 115 (2017) 500–512.
[12] P.F. Peterson, V.E. Schrock, T. Kageyama, Diffusion layer theory for turbulent vapor condensation with noncondensable gases, J. Heat Transf.-Trans. ASME 115 (1993) 998–1003.
[13] T. Kageyama, P.F. Peterson, V.E. Schrock, Diffusion layer modeling for condensation in vertical tubes with noncondensable gases, Nucl. Eng. Des. 141 (1993) 289–302.
[14] C.Y. Warner, V.S. Arpaci, An experimental investigation of turbulent natural convection in air at low pressure along a vertical heated flat plate, Int. J. Heat Mass Transf. 11 (3) (1968) 397–406.
[15] F. Blangetti, R. Krebs, E. Schlunder, Condensation in vertical tubes-experimental results and modeling, Chem. Eng. Fundam. 1 (2) (1982) 20–63.
[16] H.J.H. Brouwers, Effect of fog formation on turbulent vapor condensation with noncondensable gases, J. Heat Transf.-Trans. ASME 118 (1) (1996) 243–245.
[17] S. Oh, S.T. Revankar, Experimental and theoretical investigation of film condensation with noncondensable gas, Int. J. Heat Mass Transf. 49 (15–16) (2006) 2523–2534.
[18] E.M. Sparrow, S.H. Lin, Condensation heat transfer in the presence of a noncondensable gas, J. Heat Transf. 86 (3) (1964) 430–436.
[19] W. Minkowycz, E. Sparrow, Condensation heat transfer in the presence of noncondensables, interfacial resistance, superheating, variable properties, and diffusion, Int. J. Heat Mass Trans. 9 (1966) 1125.
[20] J.W. Rose, Condensation of a vapour in presence of a non-condensing gas, Int. J. Heat Mass Transf. 12 (2) (1969) 233.
[21] X. Wu, T. Li, Q. Li, F. Chu, Approximate equations for film condensation in the presence of non-condensable gases, Int. Commun. Heat Mass Transf. 85 (2017) 124–130.
[22] R. Savino, D. Paterna, Marangoni effect and heat pipe dry-out, Phys. Fluids 18 (2006) 118103.
[23] R.W. Schrage, A Theoretical Study of Interface Mass Transfer, Columbia University Press, New York, 1953.
[24] T. Qin, R.O. Grigoriev, The effect of noncondensables on buoyancy-thermocapillary convection of volatile fluids in confined geometries, Int. J. Heat Mass Transf. 90 (2015) 678–688.
[25] T. Qin, Ž. Tuković, R.O. Grigoriev, Buoyancy-thermocapillary convection of volatile fluids under atmospheric conditions, Int. J. Heat Mass Transf. 75 (2014) 284–301.
[26] T. Qin, Ž. Tuković, R.O. Grigoriev, Buoyancy-thermocapillary convection of volatile fluids under their vapors, Int. J. Heat Mass Transf. 80 (2015) 38–49.
[27] R.O. Grigoriev, T. Qin, The effect of phase change on stability of convective flow in a layer of volatile liquid driven by a horizontal temperature gradient, J. Fluid Mech. 838 (2018) 248–283.
[28] Y. Li, R.O. Grigoriev, M. Yoda, Experimental study of the effect of noncondensables on buoyancy-thermocapillary convection in a volatile low-viscosity silicone oil, Phys. Fluids 26 (2014) 122112.
[29] Y. Kataoka, T. Fukui, S. Hatamiya, T. Nakao, M. Naitoh, I. Sumida, Experiments on convection heat transfer along a vertical flat plate between pools with different temperatures, Nucl. Technol. 99 (3) (1992) 386–396.
[30] H. Uchida, A. Oyama, Y. Togo, Evaluation of post-incident cooling systems of light water power reactors, tech. rep., Tokyo Univ., 1964.